V. TETYORKIN, Z. TSYBRII, V. SLIPOKUROV,
A. YEVMENOVA, K. ANDRIEIEVA, O. KOSULYA

V.E. Lashkaryov Institute of Semiconductor Physics, Nat. Acad. of Sci. of Ukraine
(41, Nauky Ave., Kyiv 03028, Ukraine)

MODELING OF THE MECHANISMS OF CHARGE CARRIER TRANSPORT IN HgCdTe AND InSb PHOTODIODES IN THE 3–5-μm SPECTRAL INTERVAL

An important problem for HgCdTe and InSb photodiodes is the excess dark current, which dominates at operating reverse bias voltages and exceeds the generation-recombination current in the space charge region. As a rule, the excess current has the bulk and surface components and causes the 1/f-type low-frequency noise, which affects the ampere-watt sensitivity and detectivity of photodiodes. In most performed studies, the tunnel nature of the excess current and its connection with the manufacturing technology of initial materials and photodiodes are noted. Using theoretical models, dark current calculations have been performed, and their results have been compared with experimental results obtained from the studies of photodiodes based on epitaxial films of p-Hg$_{1-x}$Cd$_x$Te (x ≈ 0.3) and single crystals n-InSb. A conclusion is drawn that the structure of the sensitive region in photodiodes manufactured making use of ion implantation and diffusion methods is more complicated than that in existing models. Therefore, the latter can be used as a first approximation for the qualitative and quantitative explanations of experimental results.

K e y w o r d s: IR photodiodes, HgCdTe, InSb, charge carrier transport mechanisms, dark current simulation.

1. Introduction

HgCdTe and InSb photodiodes, together with PbS and PbSe photoresistors, pyroreceivers, bolometric devices, and quantum gratings, are widely used for the registration of infrared (IR) radiation in a spectral interval of 3–5 μm [1–3]. In the cases of both single photodiodes and multi-element matrices, there exists the problem of identification of excess currents, which are associated with defects in the initial materials, as well as defects that were formed in the process of manufacture of those devices.

A challenging problem aimed at reducing the magnitude of surface currents in photodiodes is the pas-

sivation and protection of the photodiode surface. In photodiodes with an asymmetric structure of the sensitive area (of the n^+-p type for HgCdTe photodiodes, and the p^+-n type for InSb ones), a charge of only one polarity can be in-built into the passivation coating. This charge ensures the band bending in the majority carrier depleted space charge region (SCR). However, when those photodiodes are fabricated using the diffusion or ion implantation method, the doping can be symmetrical, so the application of the same passivation coating for the p- and n-regions of the junction is problematic and requires a separate analysis and research.

An important problem of the HgCdTe photodiode technology is the high concentration of dislocations at the heterojunction between the CdTe (or CdZnTe) substrate and the HgCdTe epitaxial layer, despite the matching of their lattice constants [4]. Later, such defects become a source of the excess current in p-n junctions. Therefore the parameters of photodiodes strongly depend on their manufacturing technology [5].

Another challenging problem is the elucidation of the nature of the shunt resistance of p-n junctions. It can be caused by surface and bulk defects, for example, dislocations crossing the SCR.

In spite of the fact that the existing theoretical models of the charge transfer are substantially simplified, their analysis makes it possible to highlight the problems that exist for real p-n junctions. Therefore, the aim of the work was to analyze the abovementioned problematic issues in relation to HgCdTe and InSb photodiodes and their possible solutions.

2. Experimental Specimens and Techniques

Single crystal films of $Hg_{1-x}Cd_xTe$ ($x \approx 0.3$) were grown making use of the liquid phase epitaxy method on $Cd_{1-y}Zn_yTe$ ($y \approx 0.04$) substrates from a Te-enriched melt [6]. The thickness of HgCdTe epitaxial layers was about 15–20 μm. According to the Hall effect measurements, the obtained films with p-type conductivity were characterized by the carrier concentration $N_p(77 \text{ K}) = (1 \div 3) \times 10^{16}$ cm^{-3} and mobility $\mu_p = 405$ cm^2/(V·s). Before the photodiode manufacturing process, the chemical composition (the parameter x) in $Hg_{1-x}Cd_xTe$ epitaxial layers was controlled using IR Fourier spectroscopy. The variations of x did not exceed $\Delta x \leq 0.001$.

Planar n-p junctions were formed by implanting B$^+$ ions with energies of 80–100 keV into HgCdTe epitaxial layers to doses of $(2 \div 3) \times 10^{13}$ cm^{-2}. The measurements of the electrophysical parameters of the specimens after the implantation showed that irradiation with B$^+$ ions led to the conversion of the conductivity type from p- to n-one with the formation of a highly doped n^+-layer at the material surface owing to the generation of radiation defects. The Hall concentration of electrons in this case was $N_e(77 \text{ K}) = 8.4 \times 10^{17}$ cm^{-3}, and their mobility was $\mu_p = 2.3 \times 10^3$ cm^2/(V·s). After implanting boron ions in the indicated modes, their distribution profiles into the specimen depth had a Gaussian shape with a maximum at 365 nm.

Standard photolithographic processes were used to form the desired topology of the multi-element structure, with a sensitive element size of 50×50 μm^2. Chemical treatments during the manufacturing process of HgCdTe-based IR photodiodes were carried out using bromine-containing herbicides. Two-layer Mo/In metal contacts were formed using the magnetron and thermal sputtering methods at room temperature.

Diffusion of Cd atoms into single-crystalline n-InSb substrates was carried out in three ways: isothermal, two-temperature, and combined [7]. The best results were obtained for the combined method, which was implemented in two stages. At the first stage, cadmium diffusion was carried out at a temperature of 380 °C for 1.5 h. At the second stage, the specimens were thermally annealed in vacuumed quartz ampoules at a temperature of 420 °C for three hours and, in the absence of the diffusant, in the ampoules. A certain amount of crushed Sb was additionally introduced into the ampoule in order to create a saturated Sb vapor in the free volume and avoid the Sb over evaporation from the substrate surface.

The p-n junction depth was determined by monitoring a change in the thermoelectric signal during the layer-by-layer etching of the doped layer at the mesostructure fabrication stage. The average hole concentration in the doped layer was determined from the measurements of the differential Hall effect before and after the impurity diffusion. In the doped layer 0.5 μm in thickness, it was found to be equal to $(7 \div 10) \times 10^{17}$ cm^{-3} at 77 K.

The formation of the mesostructure of the area $A = (10^{-2} \div 10^{-3})$ cm^2 was carried out using a bromine-containing etchant. After the etching, the mesostructure was passivated in an aqueous or alcoholic solution of Na$_2$S. The surface was protected by applying a polycrystalline layer of CdTe. The procedures of surface passivation and protection in HgCdTe and InSb photodiodes are described in detail in work [8]. The In-Zn alloy with the 3% zinc content was used as a contact with p-InSb, and pure In as a contact with n-InSb.

3. Modeling of Charge Transfer Mechanisms in InSb and HgCdTe Photodiodes

Since the limiting parameters and characteristics of photodiodes are largely determined by the dark current level, the considerable attention has been paid to the study of charge transfer mechanisms [1, 9]. In the general case, the dark current in a photodiode is induced by the processes of generation and tunneling of charge carriers in the bulk, SCR, and surface of the semiconductor, and it can be represented as the sum

of the diffusion, I_{D}, generation-recombination, I_{GR}, band-to-band tunneling, I_{BTB}, generation-tunneling (trap-assisted tunneling), I_{TAT}, and shunt, I_{SH}, currents,

$$I = I_{\mathrm{D}} + I_{\mathrm{GR}} + I_{\mathrm{BTB}} + I_{\mathrm{TAT}} + I_{\mathrm{SH}}. \qquad (1)$$

Except for the diffusion current, the other components in Eq. (1) can possess the bulk and surface components. Since each current component in formula (1) has a specific dependence on the applied voltage and the temperature, this fact is used to identify the charge carrier transport mechanisms.

According to Shockley [10], the diffusion current flows in an ideal p-n junction due to the bulk generation of charge carriers. The corresponding current-voltage characteristic (CVC) is described by the Shockley formula

$$I = I_0 \left[\exp \left(-\frac{qU}{kT} \right) - 1 \right].$$

At reverse biases, the saturation current I_0, which is independent of the bias, flows through the junction. The temperature dependence of I_0 has an activation character, and the activation energy ΔE is close to the band gap width E_g, since $I_0(T) \sim n_i^2$ [11].

According to the Shockley–Reed–Hall (SRH) theory, the generation and recombination of charge carriers in the SCR occurs through a level in the band gap and is most effective if this level is located near the middle of the bandgap [12]. In this case, the CVC is described by the formula

$$I = I_0 \left[\exp \left(-\frac{qU}{\beta kT} \right) - 1 \right],$$

where the ideality factor $\beta \approx 2$. For a sharp p-n junction, the generation current $I_0 = q n_i W A / \tau_0$ increases proportionally to $U^{1/2}$ because of the SCR expansion. If we neglect the weak temperature dependence on the SCR width W and the effective generation time τ_0, the activation energy for the generation current is approximately equal to $E_g/2$.

Unlike the sharp p-n junction, the smooth one is a better approximation to real junctions. As a rule, in ion-implanted and diffused p-n junctions, the spatial distribution of the doping impurity is described by the error, exponential, or linear function. In this case, the structure of the sensitive region in the p-n junction

may differ substantially from that in the sharp junction. The formation of junctions of the p^+-p^--n^--n type was experimentally established for InAs photodiodes [13]. Namely, a compensated region about 3 μm in thickness was formed, in which the concentrations p^- and n^- of charge carriers were an order of magnitude lower than in the original material with the n-type conductivity.

A linear distribution of the doping impurity concentration in diffused InSb photodiodes was found when studying the barrier capacity [14]. The formation of structures of the n^+-n^--p^--n and n^+-p^--n types in long-wavelength HgCdTe photodiodes produced using the ion implantation method was reported in works [15, 16]. The hole concentration in the compensated region was about two orders of magnitude lower in comparison with a concentration of about 10^{16} cm^{-3} in the original epitaxial films. The generation current in the smooth junction changes according to the power law $I_0 \sim U^{1/3}$, and its temperature dependence is the same as for the sharp junction.

To calculate the band-to-band tunneling current, the formula for a triangular barrier is applied [11],

$$I_{\mathrm{BTB}} = \frac{\sqrt{m} q^3 F U A}{4 \pi^2 \hbar^2 E_g^{1/2}} \exp \left[-\frac{4\sqrt{2m} E_g^{3/2}}{3 q \hbar F} \right], \qquad (2)$$

where $m^{-1} = m_e^{-1} + m_{lh}^{-1}$ is the inverse effective tunneling mass; m_e and m_{lh} are the effective masses of the electron and the light hole, respectively; F is the electric field strength in the junction; U is the applied voltage; and A is the junction area. The tunnel transparency for the parabolic barrier differs only by a numerical factor from the expression in the square brackets. If the shape of the potential barrier in the junction has little effect on the band-to-band tunneling current [17], the fluctuations of the electric field induced by the non-uniform distribution of the alloying impurity can have a critical effect. The reason for this is the exponential dependence of the barrier tunnel transparency on the electric field created by impurities [18]. The tunnel breakdown voltage characterizes the junction inhomogeneity degree, i.e., its quality. As a rule, in inhomogeneous junctions, the value of this parameter is smaller in comparison with that for homogeneous junctions and varies from specimen to specimen.

At forward and reverse bias voltages of about kT/q, the dark current depends linearly on the volt-

age. Therefore, in the equivalent circuit, the photodiode is represented as a shunt resistance R_{Sh}, the current through which is described by Ohm's law $I_{\text{Sh}} = U/R_{\text{Sh}}$ [19]. The shunt resistance determines the value of the photodiode dynamic resistance at the zero bias, and therefore the photodiode detection capability. Experimentally, R_{Sh} is determined as the maximum value of the derivative dU/dI with respect to the bias voltage U.

The nature of the shunt current has not been definitively established. However, this current is believed to mainly arise because of the surface leakage current, as well as dislocations that cross the SCR of the p-n junction. The leakage current is induced by the process of thermal generation and recombination of charge carriers with the participation of surface defects, whereas the dislocation current has the tunneling origin [20].

3.1. Generation-tunneling current with trap assistance

The trap-assisted tunneling (TAT) current model was developed to explain the "soft" breakdown in long-wavelength photodiodes fabricated on the basis of $\text{Hg}_{1-x}\text{Cd}_x\text{Te}$ ($x \approx 0.2$) solid solutions [17, 21]. It is assumed that there exist such trap levels in the band gap through which the thermal and tunnel generation of electron-hole pairs takes place in the SCR. In contrast to the recombination defect in the SRC, the trap is characterized by a substantially larger capture coefficient of minority charge carriers in comparison with that of majority ones. In the case of HgCdTe with the p-type conductivity, typical values of the ratio between the electron and hole capture coefficients are $C_n/C_p \approx 10^2$ [22].

The generation of charge carriers is considered as a two-stage transition of electrons from the valence band onto the trap level E_t followed by their transition into the conduction band. According to the SRH statistics, the rates of thermal generation of holes and electrons equal $C_p p_1$ and $C_n n_1$, respectively, where

$$n_1 = N_c \exp\left(-\frac{E_t}{kT}\right), \quad p_1 = N_v \exp\left(-\frac{E_g - E_t}{kT}\right),$$

and N_c and N_v are the effective densities of states in the conduction and valence bands, respectively. Note that, for both considered semiconductors, the quantities N_v and $C_p p_1$ determine heavy holes, the effective

mass of which in HgCdTe equals $m_{hh} = = 0.55 m_0$, where m_0 is the free electron mass [1]. The rates of hole, $\omega_v N_v$, and electron, $\omega_c N_c$, generation via the "band–trap" tunnel transitions are determined by the formulas [17, 21, 23]

$$\omega_v N_v = \frac{\pi^2 q m_{lh} F M^2}{h^3 (E_g - E_t)} \exp\left[-\frac{4\sqrt{2m_{lh}}(E_g - E_t)^{3/2}}{3q\hbar F}\right],$$
$$(3)$$

$$\omega_c N_c = \frac{\pi^2 q m_e F M^2}{h^3 E_t} \exp\left[-\frac{4\sqrt{2m_e} E_t^{3/2}}{3q\hbar F}\right], \quad (4)$$

where the trap energy E_t is reckoned from the bottom of the conduction band.

The essential difference between the rates of thermal and tunnel generation consists in that the latter exponentially depends on the applied bias voltage and can vary in wide limits. The matrix element M for the "trap-band" tunnel transition is calculated according to the formula [23]

$$M = \frac{2\hbar^2 \sqrt{2\pi}}{m_0} \left(\frac{2m_0}{\hbar^2}\right)^{1/4} \frac{E_g}{E_t^{1/4}}. \quad (5)$$

In the general case, the TAT current through a reverse-biased junction is described by the formula [1]

$$I_{\text{TAT}} = \frac{qW N_t A}{\frac{1}{\omega_v N_v + C_p p_1} + \frac{1}{\omega_c N_c + C_n n_1}}, \quad (6)$$

where N_t is the concentration of deep centers involved in tunneling. Since there are light and heavy holes in the valence band of HgCdTe and InSb, the effective masses of electrons, m_e, and light holes, m_{lh}, which are considered to be equal, were used in expressions (3) and (4). The contribution made by heavy holes to the tunneling current is usually neglected due to the low probability of their tunneling.

Several models have been developed to analyze the mechanisms of charge carrier transport in long-wavelength, $\lambda = (8 \div 12)$ μm), HgCdTe n^+-p photodiodes. The most often used was the model of one level located near the middle of the forbidden zone [24]. In this case, $\omega_c N_c = \omega_v N_v$, so the tunneling process is the most probable.

The authors of work [25] considered three possible mechanisms of TAT current running in long-wavelength HgCdTe photodiodes at a large reverse bias, when the valence band edge in the p-part of the

junction is above the conduction band edge in the n-part. The purely tunneling component prevails if the level is located near the middle of the bandgap and the thermal generation of the carriers can be neglected (e.g., at low temperatures). If the level is shifted from the middle of the bandgap, the TAT current has a tunneling and a thermal component. If the level is in the lower half of the bandgap, electrons from the valence band, at the first stage, move to the trap level via tunneling transitions; afterwards their activation transition to the conduction band takes place. In this case, the rate of tunnel current generation prevails over the thermal one. If the level is in the upper half of the bandgap, the sequence of transitions is opposite: first, the activation transition from the valence band onto the level takes place; afterwards the tunnel transition into the conduction band occurs. In this case, the rate of heat generation prevails. It is evident that if the rates of thermal and tunnel generations are close by value, it is necessary to correctly estimate their partial contributions to the total current in the p-n junction.

A detailed analysis of the conditions under which the thermal and tunnel generations are implemented in long-wavelength HgCdTe photodiodes was made in work [26]. Depending on the possible types of thermally induced and tunneling transitions, the cited authors distinguish four groups of traps (marked a, b, c, and d).

(a) The traps of this group exchange charge carriers with the valence band via thermally induced transitions, and with the conduction band via thermally induced and tunnel transitions.

(b) For the traps of this group, only thermally induced transitions are realized, as it occurs in the SRH theory.

(c) For the traps of this group, their exchange with the valence band occurs via both thermally induced and tunneling transitions, and with the conduction band via only thermally induced ones.

(d) For the traps of this group, all types of thermally induced and tunneling transitions are possible.

Besides the models with a single trap level, models with several trap levels were also developed. In particular, for the model with two levels that lie in the lower and upper halves of the bandgap at distances of $\frac{1}{3}E_g$ and $\frac{2}{3}E_g$, respectively, from the valence band edge, a satisfactory agreement between the experimental and theoretical values of dark current was obtained in the wide intervals of temperatures, $T = (30 \div 120)$ K, and bias voltages, $U \leq 1.5$ V [27].

A TAT current model, which differs from single-level models, was developed by Nemirovsky and co-authors [22]. The model is characterized by the following features: the potential barrier has a triangular shape; the spatial distribution of traps in the SCR is uniform; the energy levels of traps are evenly distributed over the forbidden gap; and the largest contribution to the tunneling current is made by traps whose energy level E_t is close to or coincides with the Fermi level E_{F}. The last feature is principal, because it determines the dependence of the TAT current on the charge carrier concentration and the temperature, which is different from that of the band-to-band current. The transition of an electron from the valence band onto the trap level is assumed to be thermally induced, whereas its subsequent transition into the conduction band occurs via the tunneling mechanism. The corresponding generation rates in formula (6) are determined by the quantities $C_p p_1$ and $\omega_c N_c$. The described models were used to analyze experimental results obtained for HgCdTe photodiodes.

3.2. Band diagram models for HgCdTe photodiodes

For the manufacture of HgCdTe photodiodes, epitaxial films with the hole concentration $p = (1 \div 3) \times \times 10^{16}$ cm^{-3} a temperature of 77 K were used. This concentration value corresponds to the Fermi level position at the distance $E_{\mathrm{F}} - E_v = (40 \div 50)$ meV above the valence band edge. In the implanted layer, the electron concentration was about 4×10^{17} cm^{-3}, which corresponds to the Fermi level position at the distance $|E_{\mathrm{F}} - E_c| \approx 30$ meV above the conduction band bottom.

The energy band diagrams for a sharp n^+-p junction in the case of small and large reverse biases are shown in Figs. 1 and 2, respectively. In the former case, only the thermally induced and tunneling electron transitions from the valence band into the conduction one are possible. At large biases, direct tunneling electron transitions from the valence band into the conduction one are possible (see Fig. 2). In the case of degeneracy, the Burstein–Moss shift $E_{\mathrm{F}} - E_c$ must be taken into account. Therefore, direct tunneling is possible for larger reverse biases. When showing
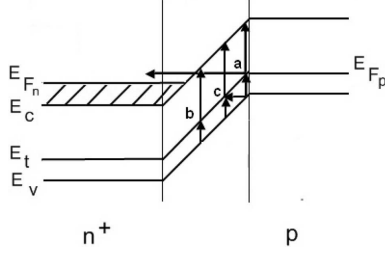
Fig. 1. Energy band diagram of the n^{+}-p junction at a small reverse bias. Vertical and horizontal arrows show possible thermally induced and tunneling, respectively, transitions for three groups of charge carriers (a, b, and c) [20]
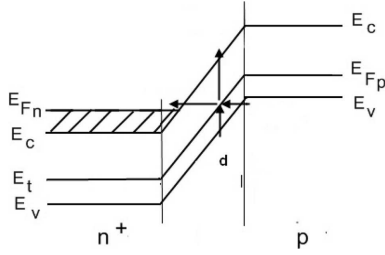
Fig. 2. Energy band diagram of the n^{+}-p junction at large reverse bias. Direct tunneling transitions from the valence band into the conduction band are possible for charge carriers of group (d)

the band diagrams, the tunneling level was assumed to lie close to the Fermi level, $E_t \approx E_{\mathrm{F}}$. According to the Fermi-Dirac statistics, it is approximately half-filled in the thermodynamic equilibrium state.

Expressions for the generation rates of the charge carriers from the indicated groups were given in work [20]. In the general case, i.e., for the traps of group (d), this formula looks like

$$U = N_t(C_nC_p(np - n_i^2) + \omega_c N_c \omega_v N_v + C_n n_1 \omega_v N_v +$$

$$+ C_p p_1 \omega_c N_c)/(C_n n_1 + C_p p_1 + \omega_c N_c + \omega_v N_v). \quad (7)$$

Expression (7) can be simplified for the other three groups of charge carriers. For example, if the trap level is located near the valence band, the conditions $n_1 \ll p_1$, $C_n n_1 \ll C_p p_1$, and $\omega_c N_c \ll \omega_v N_v$ hold. We also assume that the capture factors satisfy the condition $C_n/C_p \gg 1$, as in the case of long-wavelength HgCdTe photodiodes [22]. In particular, for the traps of group (a), the generation rate at low biases equals

$$U_a = N_t \frac{C_p p_1 \omega_c N_c}{C_c p_1 + \omega_c N_c}. \quad (8)$$
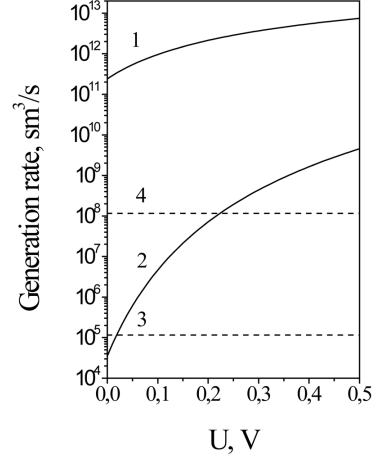
Fig. 3. Tunneling generation rates of holes, $\omega_v N_v$ (*1*), and electrons, $\omega_c N_c$ (*2*), for the trap level $E_t - E_v = 0.28E_g$. The thermally induced generation rate was calculated for $C_p = 10^{-9}$ (*3*) and 10^{-6} cm^3/s (*4*)
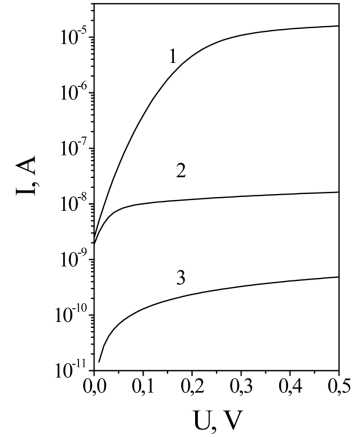

Fig. 4. Reverse CVCs calculated by formula (9) for the level $E_t - E_v = 0.28E_g$ and various $C_p = 10^{-6}$ (*1*) and 10^{-9} cm^3/s (*2*). Curve *3* is the generation current calculated according to theory [12] for the level in the middle of the bandgap

For the TAT current, we can write

$$I_{\mathrm{TAT}} = qN_t \frac{C_p p_1 \omega_c N_c}{C_p p_1 + \omega_c N_c} WA. \quad (9)$$

In formulas (7)–(9), N_t is the trap concentration from the corresponding group.

The results calculated for the generation rates and the TAT current according to formulas (3), (4), and (9) are shown in Figs. 3 and 4, respectively. The parameters of the band spectrum in HgCdTe were
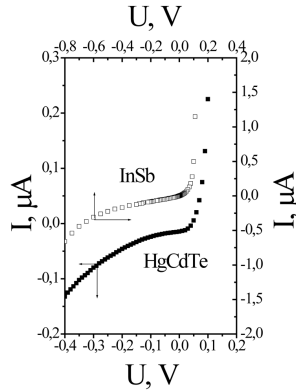
Fig. 5. CVCs of implanted HgCdTe and diffused InSb photodiodes at a temperature of 77 K
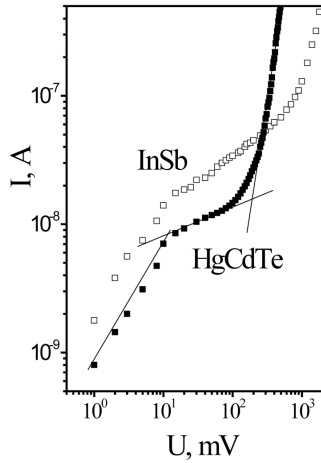
Fig. 6. Reverse CVCs for HgCdTe and InSb photodiodes at 77 K. Straight lines approximate the linear, sublinear, and exponential current dependences on the bias voltage
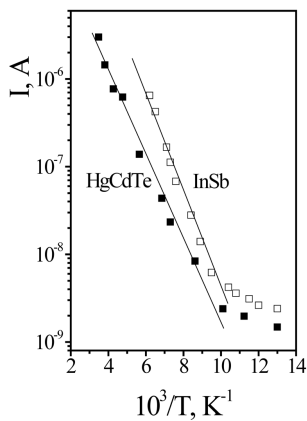
Fig. 7. Arrhenius dependences for the reverse current in the HgCdTe and InSb photodiodes at a bias voltage of 10 mV. Solid lines are drawn for averaged data

calculated according to the formulas given in Appendix. Note that, at small and medium biases, the reverse current limits the tunneling generation rate because $\omega_c N_c < C_p p_1$. At large biases, there is a tendency to current saturation as a result of its limitation by thermally induced generation. In addition, the TAT current substantially exceeds the Shockley generation current $I_0 = q n_i W A / \tau_0$ because $p_1 \gg n_i$.

4. Experimental Results and Discussion

In Fig. 5, typical CVCs of photodiodes fabricated by implanting boron ions into an epitaxial p-Hg$_{1-x}$Cd$_x$Te ($x = 0.287$) film and diffusing Cd into a single-crystalline n-InSb substrate. The so-called "soft breakdown" – i.e., the smooth current growth – at moderate reverse biases is caused by the TAT mechanism of charge transfer.

In Fig. 6, the reverse CVC curves of HgCdTe and InSb photodiodes measured at a temperature of 77 K are plotted in log-log coordinates. Three characteristic sections can be distinguished in those curves. At the biases $U \leq 10$ mV, linear current–voltage dependences are observed. If the bias increases, the linear section turns into a sublinear one, which can be approximated by the power-law dependence $I \sim U^m$ with $m \approx 0.8$ for the InSb photodiode and $m \approx 0.6$ for the HgCdTe one. At the biases $U > 250$ mV for the HgCdTe photodiode and $U > 600$ mV for the InSb one, an exponential growth of the reverse current is observed. Note that in both cases, the bias voltage at which the current growth begins depends on the technological modes of photodiode fabrication.

In Fig. 7, the temperature dependences of the reverse current (the Arrhenius dependences) measured at the fixed value of bias voltage $U = 10$ mV are shown. At temperatures $T > 120$ K, the dependences can be linearized, and the activation energy ΔE for the photodiode dark current can be determined from the curve slope. For the HgCdTe photodiode, $\Delta E = (110 \div 120)$ meV, which roughly corresponds to half the bandgap width, whereas for the InSb photodiode, $\Delta E \approx 130$ meV [28]. The deviation from the Arrhenius dependences at low temperatures is typical of IR photodiodes and is explained by the tunneling mechanism of current flow [29].

The reverse CVC dependences measured for the HgCdTe photodiode at various temperatures are shown in Fig. 8. At $T > 120$ K, the experimental

CVCs agree well with those calculated by the formula $I_0 = qn_iWA/\tau_0$ with $\tau_0 = 10^{-9}$ s (the effective generation time in the SCR, τ_0, was used as a fitting parameter, and it was assumed to be independent of the temperature). Note that, in this case, according to the theory (see work [12]), the thermal generation of charge carriers takes place with the participation of recombination defects, whose levels are located close to the middle of the bandgap.

At low temperatures, the CVCs have two sections: a sublinear one at low biases and a superlinear one at the biases larger than 250 mV. It is obvious that the former section is associated with the thermally induced generation of charge carriers, whereas the latter one is caused by tunneling. A similar behavior of reverse CVCs is typical of the InSb and InAs photodiodes and long-wavelength HgCdTe photodiodes [29, 30]. The current behavior at low biases can be satisfactorily explained if we assume that the traps of group (a) participate in heat generation, see Fig. 1. The calculation results shown in Fig. 9 were obtained using Eq. (9) with the parameter values $E_{t1} - E_v = 0.28$ mV, $E_g \approx 60$ meV, $N_{t1} = 1 \times 10^{15}$ cm^{-3}, and $C_{p1} = 10^{-9}$ cm^3/s.

Since the current with the participation of the traps from groups (b) and (c) is limited by the thermally induced electron transitions from the trap level to the conduction band (Fig. 1) and the rate $C_n n_1$ of those transitions is much lower than the rate $\omega_c N_c$ of tunneling transitions, its contribution can be neglected. Note that, at the indicated parameter values, the thermal and tunneling generation rates are close at the biasws $U < 20$ mV. At larger biases, the TAT current is limited by the thermally induced generation and increases owing to the SCR expansion (see Figs. 3 and 4). Since it is impossible to explain the experimental CVCs in the framework of the one-level model, the two-level model (one level in both the lower and upper halves of the bandgap) was used. At the biases $U > 250$ mV, purely tunneling transitions are possible from the valence band into the conduction one through the level in the upper half of the bandgap, so the TAT current can be calculated using the formula

$$I_{TAT} = qWN_tA\left(\frac{1}{\omega_v N_v} + \frac{1}{\omega_c N_c}\right)^{-1}. \qquad (10)$$

Coincidence with experimental results was obtained for the level energy $E_{t2} - E_v = 0.72$ meV,
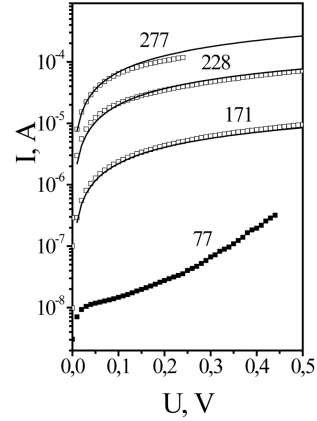
Fig. 8. Reverse CVCs for the HgCdTe photodiode at various temperatures (in kelvins). Solid lines are the results of calculations of generation current when the trap level is in the middle of the bandgap (see explanations in the text)
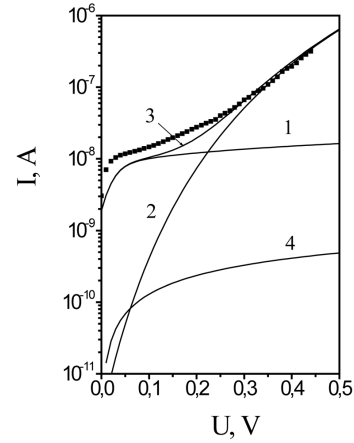
Fig. 9. Reverse CVCs for the HgCdTe photodiode at $T = 77$ K. Solid curves are the results of calculations of the TAT current according to formulas (9) and (10) for the trap levels in the lower (curve *1*) and upper (curve *2*) halves of the bandgap, and the total current (curve *3*). Curve *4* is the Shockley generation current for the level in the middle of the bandgap

$E_g \approx 160$ meV, and the trap concentration $N_{t2} \approx \approx 10^{12}$ cm^{-3}. These values correlate with those obtained for the two-level model in long-wavelength HgCdTe photodiodes [27].

In order to explain the TAT current in InSb photodiodes, a model of inhomogeneous junction was developed [13, 31]. The following assumptions were made: (i) the tunnel current is determined by the regions with an increased defect concentration, which substantially differs from the average value found from the barrier capacity measurements; (ii) the most
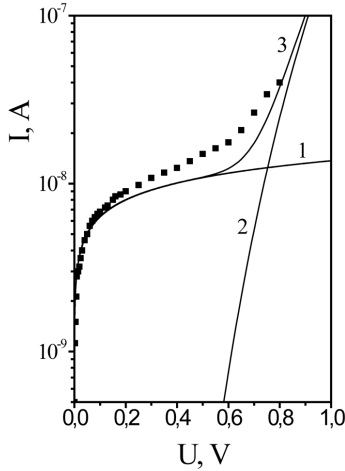
Fig. 10. Reverse CVCs for the InSb photodiode at $T = 77$ K. Theoretical CVCs correspond to the Shockley generation current (curve *1*), the TAT current with the participation of acceptor-type traps (curve *3*), and their sum (curve *3*)

probable reason for the appearance of inhomogeneous regions with an increased defect concentration is dislocations that cross the SCR; (iii) there is the so-called Cottrell atmosphere around a dislocation; it surrounds the dislocation core at a distance of several micrometers; (iv) a dislocation together with its impurity atmosphere has an effective cross-section area of 1 μm^2; and (v) the total area of inhomogeneous regions in the *p-n* junction was determined from the dislocation concentration in the initial single crystals ($\sim$10^4 cm^{-2}) and was equal to several percent of the area A of the *p-n* junction, so, their contribution in the barrier capacity can be neglected. The electric field in the inhomogeneous regions substantially exceeds its average value in the homogeneous part of the junction and stimulates the appearance of the excess TAT current. The concentration of defects in the impurity atmosphere of a dislocation was determined by fitting the calculated CVCs to experimental ones.

In the calculations, it was taken into account that the recombination SRH defects of the donor type are responsible in InSb for the recombination of non-equilibrium charge carriers, and the levels of those defects are close to the middle of the bandgap [32,33]. In InSb photodiodes, they determine the generation current $I_0 = qn_iWA/\tau_0$, and typical values of τ_0 are about 10^{-8} s [1]. In work [34], it was shown that in a wide temperature interval, the lifetime of non-equilibrium electrons and holes in *n*-InSb can be de-

scribed in the framework of a two-level model: a donor-type recombination level located in the middle of the bandgap and an acceptor-type trap level; they arise as a result of the Cd impurity diffusion into a material with the *n*-type conductivity. It was suggested that the acceptor traps are associated with dislocations in the SCR of the junction. The trap level is at a distance of about 70 meV from the conduction band bottom, and the trap concentration is about 10^{13} cm^{-3}. The influence of acceptor traps on the TAT current in InSb photodiodes has not been reported yet in the literature.

The experimental and calculated reverse CVCs are shown in Fig. 10. The calculations were performed for a junction with a linear distribution of the impurity concentration because the barrier capacity in diffused junctions can be straightened in the C^{-3} vs U coordinates. In formulas (3) and (4), the maximum value of the electric field in the junction was used,

$$F_{\max} = \frac{1.5(U_{bi} + U)}{W}, \tag{11}$$

where $U_{bi} = 0.7E_g$ is the contact potential difference, and U is the reverse bias. The SCR width equals

$$W = \frac{12\varepsilon\varepsilon_0(U_{bi} + U)}{qa}, \tag{12}$$

where a is the impurity concentration gradient, $\varepsilon = 17.9$ is the dielectric constant of InSb, and ε_0 is the electric constant. According to the results of the barrier capacity measurements, it was found that the impurity concentration gradient was about 10^{20} cm^{-4}. A satisfactory coincidence was obtained for the model where the photodiode current is a result of the thermally induced generation of charge carriers in the homogeneous part of the *p-n* junction with the participation of trap levels in the middle of the bandgap, as well as the tunneling generation of charge carriers associated with the traps whose level lies at the distance $E_t = 80$ meV below the conduction band bottom, the trap concentration equals $N_t = 10^{14}$ cm^{-3}, and the impurity concentration gradient equals $a = 2 \times 10^{21}$ cm^{-4}. It was assumed that the generation current $I_0 = qn_iWA/\tau_0$ flows through the homogeneous part of the junction with the area $A = 1.4 \times 10^{-2}$ cm^2, and the generation time τ_0 was assumed equal to 10^{-8} s. The TAT current flows through the non-uniform junction part whose total

area is 2×10^{-4} cm^2. Formula (10) was used for its calculation. Note the correlation between the values of the trap energy position found from the photoconductivity kinetics measurements and the photodiode CVCs. The differences in the trap concentration and the concentration gradient can be explained by the fact that their values in photodiodes are characterized by the SCR parameters rather than those of the initial material.

An important feature of IR photodiodes based on the narrow-gap semiconductors HgCdTe, InSb, and InAs is the dependence of the TAT current on the fabrication technology. Therefore, the reported in the literature experimental values of the parameters that determine its value and functional dependence on the applied voltage have a considerable spread. For example, in long-wavelength HgCdTe photodiodes created on substrates with close electrical parameters, the dark current fluctuations can be several orders of magnitude [30]. If p-type epitaxial films with the concentration of small acceptors $N_A \approx 10^{16}$ cm^{-3} are used, the trap concentration in photodiodes varies within the limits from $0.1 N_A$ to $10 N_A$, and the coefficient C_p, which determines the rate of thermally induced hole generation, varies from about 10^{-4} cm^3/s to about 10^{-10} cm^3/s [22, 26, 35].

Furthermore, there is no unequivocal viewpoint concerning the type of traps (acceptor or donor), as well as their nature. It was noted, however, that one of the most probable origins of the parameter spread in photodiodes, both single and located in multicomponent photodetectors, can be bulk and extended defects (extractions of another phase, precipitates, dislocations) in the SCR of the p-n junction [36]. The results obtained in this work testify to the possibility of the qualitative and quantitative analyses of the CVCs of photodiodes in the medium-wavelength interval using the theoretical models of the charge carrier transport developed for long-wavelength HgCdTe photodiodes. The body of experimental results obtained for the InSb and HgCdTe photodiodes in the medium-wavelength spectral interval is much smaller than that obtained in the long-wavelength one. Therefore, the necessity of researching their properties remains to be a challenging task.

5. Conclusions

Theoretical models of charge carrier transport in infrared photodiodes based on the narrow-gap semiconductors Hg$_{1-x}$Cd$_x$Te ($x \approx 0.3$) and InSb have been analyzed. The reverse current in photodiodes and its dependences on the applied bias voltage and the temperature are studied in a temperature interval of 77–300 K. The temperature intervals are identified where the tunneling and thermally induced mechanisms of charge carrier generation are realized. Based on the analysis of experimental data and the results of theoretical calculations, the following conclusions are drawn:

• the TAT current in photodiodes is governed by the thermally induced generation of charge carriers at the temperatures $T > 120$ K and their tunneling generation at lower temperatures;

• several levels located in the forbidden band participate in the thermal and tunneling generation of charge carriers;

• the probable origin of the TAT current is the traps associated with dislocations that cross the SCR of the p-n junction;

• there is no correlation between the dislocation concentration in the initial material and the TAT current value; so, the dislocations can be assumed to emerge at the stage of photodiode fabrication;

• for InSb photodiodes, a model of inhomogeneous junction is developed, which suggests that the TAT current appears due to the presence of areas with an increased concentration of acceptor-type traps.

APPENDIX
Band parameters for Hg$_{1-x}$Cd$_x$Te

The following approximation formulas given in monograph [1] for the dependences of the parameters of the Hg$_{1-x}$Cd$_x$Te semiconductor on its content x were used to calculate the band parameters: for the band gap width,

$$Eg(x) = -0.302 + 1.93x - 0.81x^2 + 0.832x^3 +$$

$$+ 5.3510^{-4} \times (1 - 2x),$$

for the intrinsic charge carrier concentration,

$$n_i = (5.585 - 3.82x + 0.001753T - 0.001364xT) \times$$

$$\times 10^{14} \times E_g^{3/4} T^{3/2} \exp\left(-\frac{E_g}{2kT}\right);$$

for the high-frequency dielectric permittivity,

$$\varepsilon_\infty = 15.2 - 15.6x + 8.2x^2;$$

for the static dielectric permittivity,

$$\varepsilon_0 = 20.5 - 15.6x + 5.7x^2.$$

The effective masses of electrons and light holes were assumed to be identical and equal to $m_e = m_{lh} = = 0.071 E_g m_0$, and the effective mass of heavy holes was taken to equal $m_{hh} = = 0.55 m_0$.

1. A. Rogalski. *Infrared Detectors. 2nd edition* (CRC Press, Taylor and Francis Group, 2011).

2. X. Lyu. Recent progress on infrared detectors: materials and applications. *Highlights Sci. Eng. Technol.* **27**, 191 (2022).

3. A. Rogalski, M. Kopytko, F. Dai, R. Jiang, F. Wang, W. Hu, P. Martyniuk. Infrared HOT material systems vs. law 19 paradigm. *Measurement* **230**, 114495 (2024).

4. A Sher, M.A. Berding, M. van Schilfgaarde, An-Ban Chen. HgCdTe status review with emphasis on correlations, native defects and diffusion. *Semicond. Sci. Technol.* **6**, 59 (1991).

5. *Mercury Cadmium Telluride: Growth, Properties and Applications. Edited by P. Capper and J. Garland* (Wiley, 2011).

6. Z. Tsybrii, Yu. Bezsmolnyy, K. Svezhentsova *et al.* HgCdTe/CdZnTe LPE epitaxial layers: from material growth to applications in devices. *J. Cryst. Growth* **529**, 125295 (2020).

7. A. Sukach, V. Tetyorkin, A. Voroschenko, A. Tkachuk *et al.* Carrier transport mechanisms in InSb diffused *p-n* functions, *SPQEO* **17**, 325 (2014).

8. V. Tetyorkin, Z. Tsybrii, A. Tkachuk, M. Vuichyk, K. Svezhentsova, A. Yevmenova, N. Dmytruk. Passivation of InSb and HgCdTe infrared photodiodes by polycrystalline CdTe. *J. Electron. Mater.* **52**, 7337 (2023).

9. M. Vallone, M.G.C. Alasio, A. Tibaldi, F. Bertazzi, S. Hanna, A. Wegmann, D. Eich, H. Figgemeier, G. Ghione, M. Goano. Exploring optimal dark current design in HgCdTe infrared barrier detectors: a TCAD and semianalytic investigation. *IEEE Photon. J.* **16**, 6800208 (2024).

10. W. Shockley, W.T. Read Jr. Statistics of the recombination of holes and electrons. *Phys. Rev.* **87**, 835 (1952).

11. S. M. Sze. *Physics of Semiconductors Devices. 2nd edition* (Wiley, 1981).

12. C.T. Sah, R.N. Noyce, W. Shockley. Carrier generation and recombination in *p-n* junctions and *p-n* junction characteristics. *Proc. IRE* **45**, 1228 (1957).

13. V. Tetyorkin, A. Sukach, A. Tkachuk. InAs infrared photodiodes. In: *Advanced in Photodiodes*. Edited by G.-F. Dalla Betta (INTECH, 2011), p. 427.

14. A.V. Sukach, V.V. Tetyorkin, A.I. Tkachuk. Electrical properties of InSb *p-n* junctions prepared by diffusion method. *SPQEO* **19**, 295 (2016).

15. Y. Nemirovsky, D. Rosenfeld, R. Adar, A. Kornfeld. Tunneling dark currents in HgCdTe photodiodes. *J. Vac. Sci. Technol. A* **7**, 528 (1989).

16. Y. Nemirovsky, A. Unikovsky. Tunneling and $1/f$ noise currents in HgCdTe photodiodes. *J. Vac. Sci. Technol. B* **10**, 1602 (1992).

17. I.Y. Wong. Effect of trap tunneling on the performance of long-wavelength $Hg_{1-x}Cd_xTe$ photodiodes. *IEEE Trans. ED* **27**, 48 (1980).

18. M.E. Raikh, I.M. Ruzin. Fluctuation mechanism of excess tunneling current in reverse-biased *p-n* junctions. *Fiz Tekhn. Poluprovod.* **19**, 1217 (1985) (in Russian).

19. D.K. Schroder. *Semiconductor Material and Device Characterization* (Wiley, 2008).

20. V. Gopal, S. Gupta. Effect of dislocations on the zero-bias resistance-area product, quantum efficiency, and spectral response of LWIR HgCdTe photovoltaic detectors. *IEEE Trans ED* **50**, 1220 (2003).

21. W.W. Anderson. Tunnel contribution to $Hg_{1-x}Cd_xTe$ and $Pb_{1-x}Sn_xTe$ *p-n* junction diode characteristics. *Infrared Phys.* **20**, 353 (1980).

22. Y. Nemirovsky, R. Fastow, M. Meyassed, A. Unkovsky. Trapping effects in HgCdTe. *J. Vac. Sci. Technol. B* **9**, 1829 (1991).

23. W.W. Anderson, H.J. Hoffman. Field ionization of deep levels in semiconductors with applications with $Hg_{1-x}Cd_xTe$ *p-n* junctions. *J. Appl. Phys.* **53**, 9130 (1992).

24. D.K. Blanks, J.D. Beck, M.A. Kinch, L. Colombo. Band-to-band tunnel processes in HgCdTe: Comparison of experimental and theoretical studies. *J. Vac. Sci. Technol. A* **6**, 2790 (1988).

25. R. Krishnamurthy, M.A Berding, H. Robinson, A. Sher. Tunneling in long-wavelength infrared HgCdTe photodiodes. *J. Electron. Mat.* **35**, 1399 (2005).

26. D. Rosenfeld, G. Bahir. A model of the trap-assisted mechanism in diffused and implanted n^+-*p* HgCdTe photodiodes. *IEEE Trans. ED* **39**, 1638 (1992).

27. A. Unikovskiy Y. Nemirovsky. Trap-assisted tunneling in mercury cadmium telluride photodiodes. *Appl. Phys. Lett.* **61**, 330 (1992).

28. A.V. Sukach, V.V. Tetyorkin, A.I. Tkachuk. Carrier transport mechanisms in reverse biased InSb *p-n* junctions. *SPQEO* **18**, 267 (2015).

29. V. Tetyorkin, A. Sukach, A. Tkachuk. Infrared photodiodes on II–VI and III–V narrow-gap semiconductors. In: *Photodiodes – From Fundamentals to Applications*. Edited by Ilgu Yun (INTECH, 2012).

30. A. Zemel, I. Lukomsky, E. Weiss. Mechanism of carrier transport across the junction of narrow band-gap planar n^+-*p* HgCdTe photodiodes grown by liquid-phase epitaxy. *J. Appl. Phys.* **98**, 054504 (2005).

31. A.V. Sukach, V.V. Tetyorkin, N.M. Krolevec. Tunneling current via dislocations in InAs and InSb infrared photodiodes. *SPQEO* **14**, 416 (2011).

32. R.A. Laff, H.Y. Fan. Carrier lifetime in indium antimonide. *Phys. Rev.* **121**, 53 (1961).

33. J.E.L. Hollis, C. Choo, E.L. Heasell. Recombination centers in InSb. *J. Appl. Phys.* **35**, 1626 (1967).

34. V. Tetyorkin, A. Tkachuk., I.G. Lutsyshyn. Recombination and trapping of excess carriers in *n*-InSb. *Ukr. J. Phys.* **69**, 45 (2024).

35. W. He, Z. Celik-Butler. $1/f$ noise and dark current components in HgCdTe MIS infrared detectors. *Solid-State Electron.* **39**, 127 (1996).

36. I.M. Baker, C.D. Maxey. Summetry of HgCdTe 2D array technology in the U.K. *J. Electron. Mater.* **30**, 682 (2001).

В. Тетьоркін, З. Цибрій, В. Сліпокуров,
А. Євменова, К. Андреєва, О. Косуля

МОДЕЛЮВАННЯ МЕХАНІЗМІВ ТРАНСПОРТУ
НОСІЇВ ЗАРЯДУ В HgCdTe ТА InSb ФОТОДІОДАХ
НА ДІЛЯНКУ СПЕКТРА 3–5 мкм

Важливою проблемою для HgCdTe та InSb фотодіодів є надлишковий темновий струм, який домінує при робочих напругах зворотного зміщення і перевищує генераційно-рекомбінаційний струм в області просторового заряду (ОПЗ). Як правило, надлишковий струм має об'ємну та поверхневу складову і зумовлює низькочастотний шум $1/f$-типу, який впливає на ампер-ватну чутливість та виявлювальну здатність фотодіодів. У більшості виконаних досліджень відзначається тунельна природа надлишкового струму і зв'язок з технологією виготовлення вихідних матеріалів та фотодіодів. З використанням теоретичних моделей виконано розрахунки темнового струму, які співставлені з експериментальними результатами, отриманими із досліджень фотодіодів на основі епітаксійних плівок *p*-Hg$_{1-x}$Cd$_x$Te ($x \sim 0{,}3$) та монокристалів *n*-InSb. Зроблено висновки про те, що структура чутливої області у фотодіодах, виготовлених методами іонної імплантації та дифузії, більш складна, ніж у існуючих моделях, тому останні можна використати як перше наближення для якісного і кількісного пояснення експериментальних результатів.

Ключові слова: ІЧ фотодіоди, HgCdTe, InSb, механізми транспорту носіїв заряду, моделювання темнового струму.